Research Article | Vol. 30, No. 12 / 6 Jun 2022 / Optics Express 20532
Optics EXPRESS

# Polarization-selective absorptive and transmissive metamaterials

XIAOYAN SHI,[1,2,3,4] ZHENG QIN,[1,2,3,4] ZHONGZHU LIANG,[1,2,3,*] DEJIA MENG,[2] JINHUAN LI,[1] SHOUTAO ZHANG,[1] RUI DAI,[1] ENZHU HOU,[1] WEI XIN,[1] HUA LIU,[1] HAIYANG XU,[1] AND YICHUN LIU[1]

[1] *Center for Advanced Optoelectronic Functional Materials Research and Key Laboratory of UV Light-Emitting Materials and Technology of Ministry of Education, College of Physics, Northeast Normal University, Changchun 130024, China*
[2] *State Key Laboratory of Applied Optics, Changchun Institute of Optics, Fine Mechanics and Physics, Chinese Academy of Sciences, Changchun, Jilin, 130033, China*
[3] *University of the Chinese Academy of Sciences, China*
[4] *Xiaoyan Shi and Zheng Qin contributed equally to this work*
[*] *liangzz@nenu.edu.cn*

**Abstract:** A polarization sorting metamaterial with polarization filtering and absorption is proposed. When unpolarized incident light strikes the metamaterial, one polarization component is completely absorbed, and the other polarization component is completely transmitted. We achieved an absorption extinction ratio of up to 350 and a transmission extinction ratio of 425 simultaneously in the LWIR. Unlike the 50% energy utilization limit of other polarization absorbers due to the complete reflection of another polarization component, our proposed metamaterial can be composed of layered polarization selective absorption devices to achieve more than 90% energy utilization. Therefore our design can provide a new solution for real-time polarization detection.



## 1. Introduction

Metamaterials are a powerful platform to manipulate the amplitude, phase, and polarization of light at subwavelength scales [1,2]. Metamaterials can achieve functions that are difficult to achieve by natural materials, such as negative refractive index [3], induced transparency [4], metalens [5], stealth cloak [6], and near field enhancement [7], and perfect absorption [8]. Among them, metamaterial absorbers have received extensive attention because they can achieve perfect absorption at any target wavelength through rational geometric parameters. Since Landy et al. first proposed and demonstrated a metamaterial absorber working in the microwave band in 2008 [9], perfect absorption based on the metal-dielectric-metal sandwich metamaterial structure has been achieved in wavelengths varying from microwave to visible light [8,10,11]. Metamaterial absorbers can confine the incident light field to a spatial scale much smaller than the wavelength, resulting in local hot spots and perfect absorption within a minimal thickness [12]. It shows applications in solar energy absorption [13], thermal emitters [14], photodetectors [15], and optical sensing [16,17], radiative cooling [18].

Previous metamaterial absorbers always focus on their spectral response range and sensitivity to the incident angle. To maximize the utilization of incident light energy, rotationally symmetric patterns are often used to obtain polarization-insensitive absorption [8]. In recent years, polarization-sensitive absorption has begun to receive significant attention with the development of polarization imaging and polarization detection technology [19–22]. Compared with polarization filters, polarization gratings, and other devices that require additional assembly, the metamaterial absorber with polarization selection can be directly integrated into the device with a smaller size and compact structure. Many reports have used asymmetric resonators to achieve linear

#456849 https://doi.org/10.1364/OE.456849
Journal © 2022 Received 28 Feb 2022; revised 22 Apr 2022; accepted 22 Apr 2022; published 24 May 2022

Optics EXPRESS

polarization selective absorption and circular polarization selective absorption [23–25]. However, the extinction ratio of polarization selective metamaterial absorbers realized by asymmetric patterns is generally too low to meet the needs of applications. Absorbers using one-dimensional grating patterns can obtain a high extinction ratio [26–28], and a broad wavelength band's polarization-selective absorption can be achieved using combined gratings with multiple widths. For example, the multilayer dielectric-metal grating structure proposed by Liu Zhang et al. achieves polarization-selective absorption of three peaks in the mid-and long-wave infrared [28]. Yan Kai Zhong et al. proposed an integrated aluminum grating on a multilayer stacked metal-dielectric layer, which achieved a broadband absorption in the wavelength range of 1.98-11.74 μm [27]. To the best of our knowledge, the strategy to achieve polarization-selective absorption in existing reports is to absorb one polarization component of the incident light and reflect the other polarization component. This also means that we cannot obtain information on both polarization components in a beam of light simultaneously, and the limit of energy utilization is less than 50%. In the polarization detector, absorbers with multiple polarization directions need to be placed on a plane [29,30], which sacrifices the spatial resolution.

Here we propose a metamaterial that can simultaneously achieve polarization absorption and transmission. When the unpolarized incident light reaches the surface of the metamaterial, the TM component (polarization direction parallel to the cut-wire) of incident light coupled with the cut-wire resonator is completely absorbed. The TE component (perpendicular to the cut-wire resonator) is transmitted through the metamaterial, which can be further absorbed by the below layer and utilized. The absorption extinction ratio of our metamaterial at the target wavelength can reach 380, the transmission extinction ratio can reach 425. Furthermore, we demonstrate that polarization-selective absorption and transmission over a broad spectral range can be achieved by adopting the structure of stacking multiple resonators in combination. Unlike the function switching of absorption and transmission realized by phase change materials such as vanadium oxide [31–34], our proposed metamaterial can realize real-time polarization-selective absorption and transmission. It may have promising applications for infrared polarization detection. For example, we can use layered focal planes to obtain real-time information on both polarization directions, enabling high-resolution real-time polarization detection.

## 2. Single wavelength polarization selective absorption and transmission

### 2.1. Design and modeling

As shown in Fig. 1, our proposed metamaterial consists of a three-layer structure of cut-wire resonator array-dielectric layer-subwavelength metal grating. Each period of subwavelength metal grating contains one wire pair. The following geometric parameters characterize the structure of the metamaterial: The length (x-axis) and width (y-axis) of the cut-wire resonator are denoted by $L$ and $W_1$, and the period is $P_x$ and $P_y$. The period (y-direction) of the subwavelength metal grating $P_1$, the width of the wire is $W_2$, and the gap of the wire pair is $g$. The thickness of resonator, dielectric and grating layers are denoted by $t_1$, $t_2$, and $t_3$. The metal here is aluminum (Al), and the dielectric layer is zinc selenide (ZnSe). We chose aluminum because its optical properties are comparable to noble metals (gold) in infrared wavebands at a lower cost. Zinc selenide is a commonly used infrared glass material. In our simulation band, $n_{ZnSe} = 2.36\sim2.41$. Compared with silicon and germanium, it has a lower refractive index, higher transmittance and has no absorption in the long-wave infrared band.

To characterize the performance of the metamaterial, we performed a simulation using the finite-difference time-domain (FDTD) method. The material parameters of aluminum and zinc selenide were obtained from Rakic [35] and Querry [36], respectively. The light is incident along the negative direction of the z-axis, periodic boundary conditions are used in the x and y directions, and the PML boundary is used in the z-direction. We set the geometric parameters

Optics EXPRESS

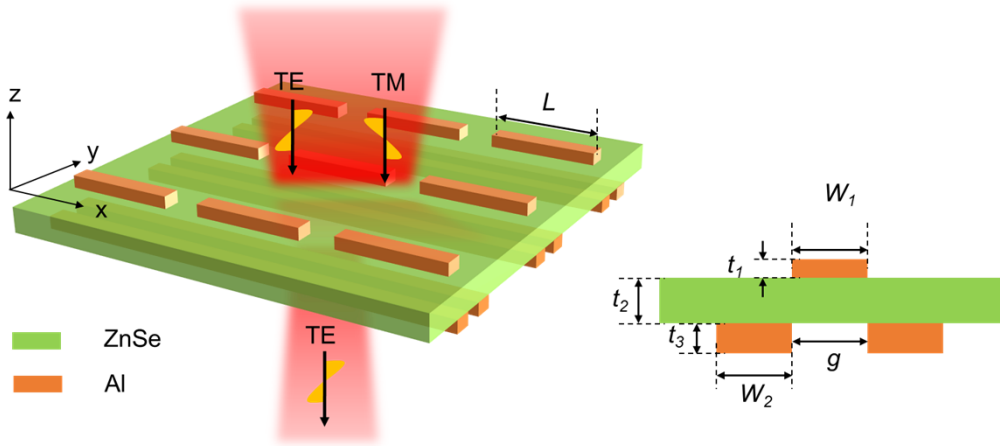


**Fig. 1.** Schematic diagram of the metamaterial

of the metamaterial as: $L = 1.8$ μm, $W_1 = W_2 = g = 0.3$ μm, $P_x = P_y = P_1 = 2$ μm. $t_1 = 50$nm, $t_2 = 150$nm, $t_3 = 100$nm.

### 2.2. Result and discussion

The optical properties of our proposed metamaterial are shown in Fig. 2. When the TM wave is incident (the incident electric field is along the x-axis direction), it behaves as a metamaterial absorber. The reflectivity at 8.85 μm is less than 0.2%, and the reflectivity at other wavelengths rises rapidly and gradually approaches 100%. When the TE wave is incident (the incident electric field is along the y-axis direction), the structure exhibits low reflection. The reflectivity in the simulated band is lower than 28%. The TM wave has almost no transmission in the entire simulated wavelength band, except for a transmission peak of about 9% at 9.6 μm caused by surface plasmon resonance. The metamaterial shows high transmission of TE waves in the whole simulation band, with a minimum transmissivity of 72%, and the transmissivity at long wavelengths is close to 95%.

The absorptivity of the metamaterial is calculated by $A = 1\text{-}R\text{-}T$. It can be seen that the TM wave has a prominent absorption peak in the simulation band, and the absorptivity at 8.85 μm reaches 94%. In contrast, the TE wave has almost no absorption, the absorptivity in the whole simulation band is less than 0.5%. We plot the metamaterial absorber's absorption spectrum (gray dashed line) with the underlying metal as a continuous layer in Fig. 2(c). It can be seen that the performance of our proposed metamaterial is comparable to that of the traditional metamaterial absorber, but only the peak position is slightly blue shifted. To evaluate the polarization-selective properties of the metamaterial, we calculated the absorption extinction ratio (defined as the ratio of TM absorption to TE wave absorption) and the transmission extinction ratio (defined as the ratio of TE wave transmissivity to TM wave transmissivity), respectively. As shown in Fig. 2(d), the absorption extinction ratio of the metamaterial reaches 380 at the absorption peak of the TM wave, and the transmission extinction ratio reaches a peak value of 425 at the wavelength of 8.34 μm, comparable to that of a grating filter. The peaks of the absorption extinction ratio and the transmission extinction ratio do not coincide. The transmission extinction ratio decreases due to the enhanced transmission of the TM wave at the absorption wavelength, but it also remains above 10.

Optics EXPRESS

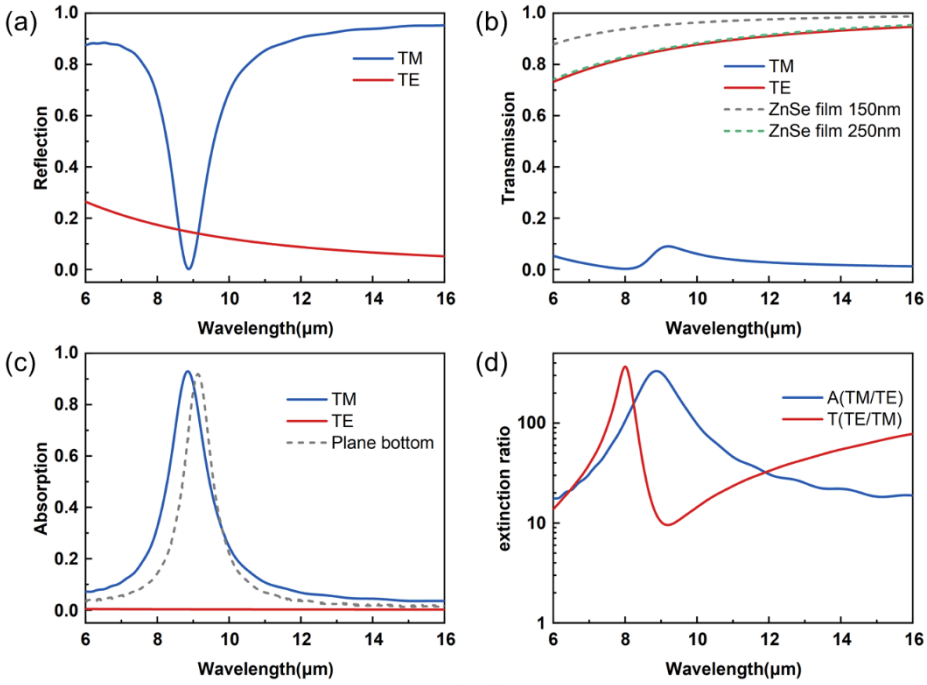


**Fig. 2.** The optical properties of our proposed metamaterial. (a) reflection spectrum, (b) transmission spectrum, (c) absorption spectrum, (d) and extinction ratio.

We calculated the equivalent impedance of the metamaterial structure to further illustrate the different responses of TM and TE waves by [37]:

$$Z = \sqrt{\frac{(1+S_{11})^2 - S_{21}^2}{(1-S_{11})^2 - S_{21}^2}} \tag{1}$$

Here $Z = Z' + iZ''$. The equivalent impedance is calculated from the scattering parameters, and the impedance of air is considered to be $Z_{air} = 1$. The real and imaginary parts of the equivalent impedance both contribute to the reflectivity of the absorber, according to $R = \frac{(Z'-1)^2+(Z'')^2}{(Z'+1)^2+(Z'')^2}$. As shown in Fig. 3(a), when the TM wave is incident, the metamaterial's impedance matches with the air at 8.85 μm, metamaterial behaves as a perfect absorber. As shown in Fig. 3(b), when the TE wave is incident, the real and imaginary parts of the equivalent impedance are almost a straight line in the entire simulation band. It shows that the metamaterial is equivalent to a transparent dielectric flat plate to the incident light.

To further illustrate the physical mechanism of polarization-selective absorption and transmission of our metamaterial, we plot the electric and magnetic field distributions at the absorption peak of the TM wave and the same wavelength of the TE wave. As shown in Fig. 4(a), when the TM wave is incident, the incident electric field couples with the upper resonator and gathers at both ends of the resonator, causing electric dipole resonance, which is consistent with the resonance of the metamaterial absorber (Fig. 4(b)). The incident magnetic field is concentrated below the resonator's dielectric layer (Fig. 4(d) and (e), thus illustrating that the physical mechanism of our proposed metamaterial TM wave absorption is consistent with that of a metamaterial absorber with a continuous metallic bottom layer [38]. Its response wavelength can be interpreted with the LC circuit model [10] as:

$$\lambda = 2\pi\sqrt{LC/2} \tag{2}$$

Optics EXPRESS

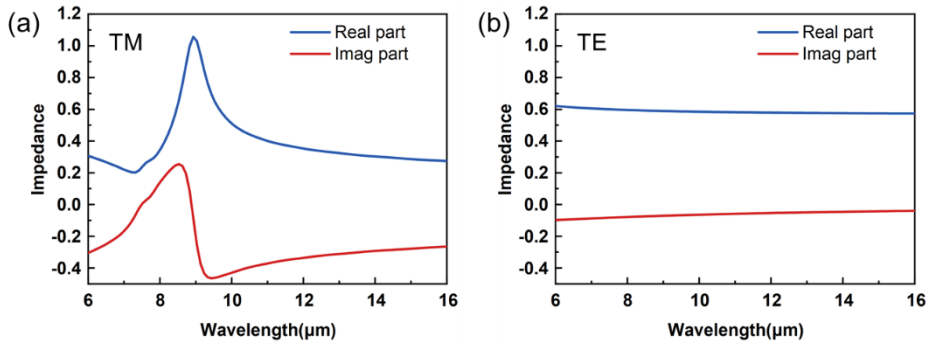


**Fig. 3.** (a) The impedance of the metamaterial under TM wave incident. (b) The impedance of the metamaterial under TE wave incident.

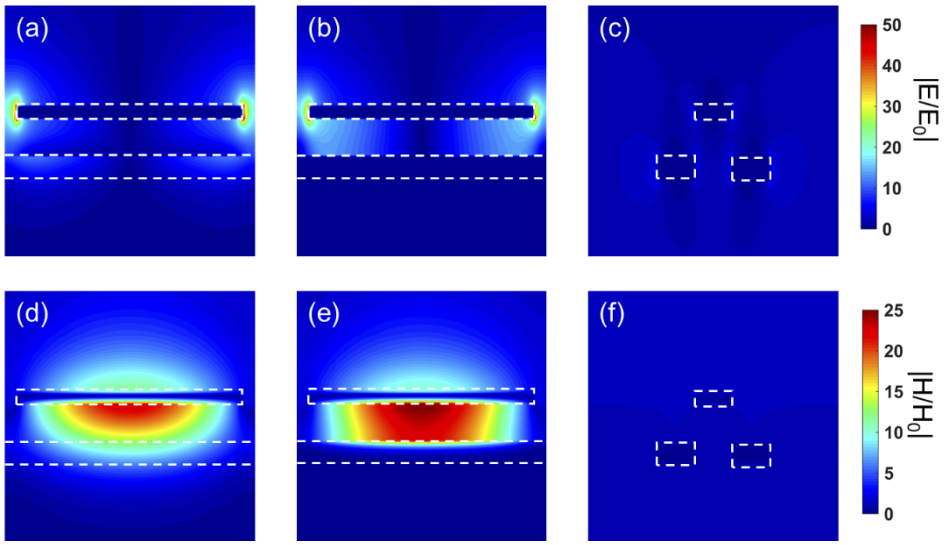


**Fig. 4.** (a) Electric field distribution at the incident absorption peak of TM wave, (b) electric field distribution at the absorption peak of metamaterial absorber with continuous metal bottom layer, (c) electric field distribution at the corresponding wavelength of TE wave incident, (d) TM wave The magnetic field distribution at the incident absorption peak, (e) the magnetic field distribution at the absorption peak of the metamaterial absorber with the continuous metal bottom layer, (f) the magnetic field distribution at the corresponding wavelength of the incident TE wave.

Here the slight blue shift of the absorption peak position of the TM wave of our metamaterial relative to the metamaterial absorber is due to the reduction of the effective relative area of the upper and lower metal layers leading to the reduction of the capacitance. For the incident TM wave, the underlying metal grating is continuous in the polarization direction of the incident optical field. Since the incident electric field is concentrated in the range of tens of nanometers at the edge of the resonator, the metal grating below the resonator can effectively act as a reflection layer for the same perfect absorption as a continuous metal layer.

For the incident TE wave, it can be seen thaneither the upper resonator nor the lower grating structure produces a surface plasmon response in the simulated band (Fig. 4(c) and (f)), thus causing no significant absorption. Due to the small duty ratio of the cut-wire resonators and the

Optics EXPRESS

bottom gratings (0.09 for the upper layer and 0.3 for the bottom layer), the metamaterial can be regarded as a single ZnSe film. As is shown by the gray dotted line in Fig. 2(b), we calculated the transmissivity of the ZnSe film using the formula [39]:

$$T = 1 - \frac{(\eta_0 - \eta_2)^2 cos^2\delta + (\eta_0\eta_2/\eta_1 - \eta_1)^2 sin^2\delta}{(\eta_0 + \eta_2)^2 cos^2\delta + (\eta_0\eta_2/\eta_1 + \eta_1)^2 sin^2\delta} \tag{3}$$

Here $\delta = \frac{2\pi}{\lambda} n_1 d \cos\theta.$, is the phase shift in the film. $\eta_0$, $\eta_{1,}$ and $\eta_2$ are the admittances of the upper dielectric of the film, the film, and the lower dielectric of the film, respectively. Due to the low refractive index of ZnSe, the transmissivity remains above 90% in the simulation band. Compared with the ZnSe film, the transmissivity of our metamaterial under TE wave drops by about 15% at short wavelengths and about 5%at long wavelengths. This is because the strong reflectivity of metal increases the effective thickness of the film. We plot the transmissivity (green dashed line) of the 250 nm thick ZnSe slab in Fig. 2(b), which almost coincides with the metamaterial's TE wave transmissivity spectrum. It shows that the upper and lower two-layer metal increases the effective thickness by about 100nm.

Therefore, we can attribute the polarization-sorting function of metamaterials to the polarization-selective surface plasmon resonance of metamaterials and the high transmittance of ZnSe thin film. When the TM wave is incident, the metamaterial excites localized surface plasmon resonance and behaves as a perfect absorber. When the TE wave is incident, the resonator does not excite surface plasmon resonance in the simulated band. The cut-wire resonators and the bottom gratings do not cause significant reflections. The metamaterial is approximated as a transparent ZnSe thin film. Therefore, our proposed metamaterial possesses high transparency (non-absorbing polarized component) that other polarized metamaterial absorbers do not have.

We examine the effect of the topography of the underlying metal grating on the performance of the metamaterial. We consider four cases in Fig. 5(a), the gap of the grating line pair is equal to the resonator width(I), smaller than the resonator width(II), larger than the resonator width(III), and only a wire grid(IV). Other parameters remain the same as above. As the gap between the grating line pairs increases, the capacitance between the upper and lower metal layers gradually decreases. Hence, the absorption peak gradually turns blue from the absorption spectrum of the TM wave in Fig. 5(b). While the transmission spectrum under TE wave incident of the three structures I, II, and III in Fig. 5(c) are almost the same because the duty cycle of the grating is not changed. For structure IV, due to the reduced duty cycle of the metal grating, the transmissivity of the TE wave is significantly higher than that of the other three structures, with a 5% increase in the whole simulation band. While for TM waves, the absorptivity drops significantly, and the transmissivity rises significantly, so the performance of polarization selection drops degraded significantly. Although the grating is located directly below the resonator, the increase in capacitance between the upper and lower metal layers red-shifts the absorption peak. Its optical field confinement ability is also significantly reduced, resulting in decreased absorptivity and increased transmissivity.

To characterize the dependence of the metamaterial's performance on the incident angle, we carried out a scanning simulation with the step length as 10° under the incident TM and TE waves, and the results are shown in Fig. 6. It can be seen in Fig. 6(a) that when the incident angle of the TM wave reaches 60°, the metamaterial still maintains more than 90% absorption. The absorption peak wavelength blue shifts with the increase of the incident angle. When the incident angle reaches 60°, the absorption peak is blue-shifted to 8.55 μm since the equivalent value of the resonator length decreases as the angle between the incident electric field component and the resonator increases. As is shown in Fig. 6(b), the transmissivity of TE wave decreases with increasing incidence angle, which follows the prediction of Eq. (3). This reduction is more pronounced at short wavelengths. When the incident angle reaches 60°, the transmissivity drops to 46% at 6 μm and 83.5% at 16 μm.

Optics EXPRESS

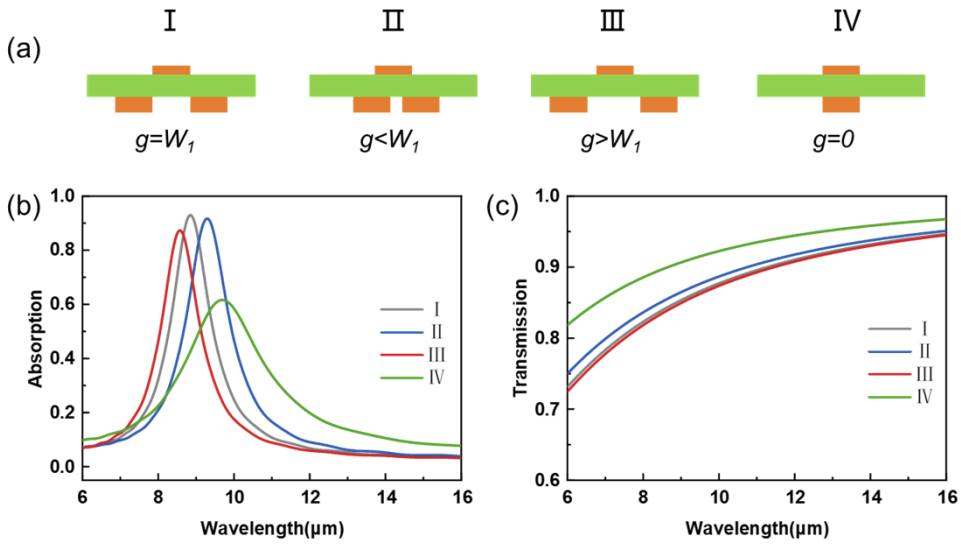


**Fig. 5.** (a) Schematic diagram of four topographies of the underlying metal grating. (b) The absorption spectrum of the four structures under TM wave incident. (c) The transmission spectrum of the four structures under TE wave incident.

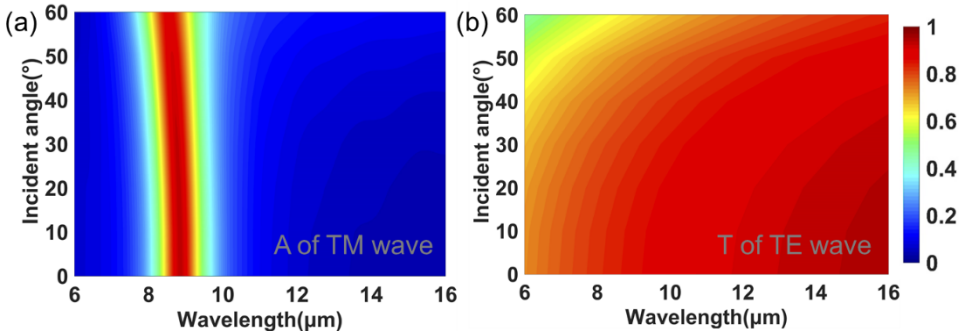


**Fig. 6.** The dependence of the metamaterial's performance on the incident angle. (a) absorption of TM wave, (b) transmission of TE wave.

Optics EXPRESS

## 3. Broadband wavelength polarization selective absorption and transmission

The high absorption of thin films for broadband infrared radiation is essential for many devices such as thermal imaging, thermal switches, etc. We try to achieve polarization-selective absorption and transmission over a broad spectral range. In Fig. 7(a), we replaced the upper single-layer resonator with a metal-dielectric-metal triple-layer structure. The period is 2.2 μm, the length of the resonator is 2 μm, the width is 0.3 μm, and a silicon nitride dielectric layer is filled between the two resonators. The thickness of the two layers of resonators is 50 nm, and the thickness of silicon nitride is 100 nm. Other parameters remain the same as above.

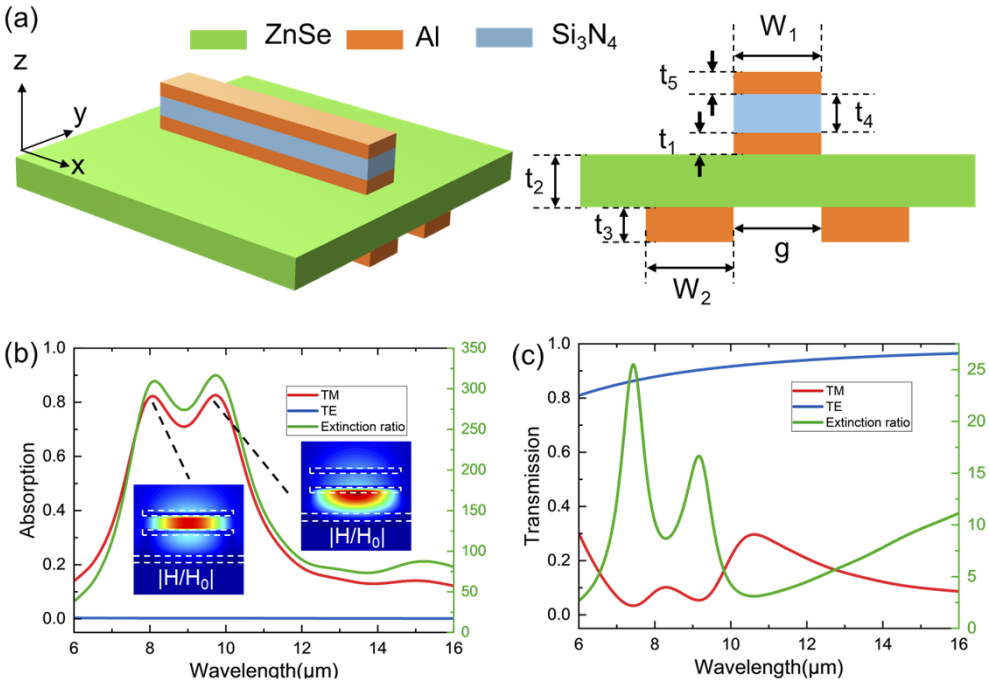


**Fig. 7.** (a) Schematic diagram of broadband polarization sorting metamaterial stacked resonator structure, (b) absorption spectrum and absorption extinction ratio (the inset is the magnetic field distribution at the two absorption peaks), (c) transmission spectrum and transmission extinction ratio.

Figure 7(b) shows the absorption spectrum and absorption extinction ratio. It can be seen that when the TM wave is incident, the absorptivity of the stacked resonator structure exceeds 70% in the wavelength range of 7.7 μm to 10.1 μm, and the absorptivity at the two absorption peaks of 8 μm and 9.8 μm wavelengths reaches 82.2% and 82.6%. When the TE wave is incident, the absorptivity of the stacked resonator structure is less than 0.3% in the whole simulation wavelength range, and the absorption extinction ratio reaches more than 250 accordingly. The average absorption extinction ratio is 293 in the broad spectral range of 7.7–10.1 μm, which is one order of magnitude higher than previously reported [27,40]. In the inset of Fig. 7(b), we plot the magnetic field distribution at the two absorption peaks. At the wavelength of 8 μm, the incident magnetic field is mainly concentrated in the silicon nitride layer between the upper and lower resonators. At the wavelength of 9.8 μm, the incident magnetic field is mainly concentrated in the zinc selenide layer between the lower resonator and the grating. It is shown that the localized surface plasmon resonance of the two resonators excited respectively induces high absorption at two wavelengths of the TM wave.

Optics EXPRESS

Figure 7(c) shows the stacked resonator structure's transmission spectrum and extinction ratio. It can be seen that under TE wave incident, the stacked resonator structure maintains high transmission in the whole simulation band, sightly high than the single resonator structure. The transmissivity of the whole simulation band remains above 80%, the transmissivity at long wavelengths reaches 96%, and the average transmissivity reaches 91.7%. When the TM wave is incident, two transmission peaks appear near the wavelengths of the two absorption peaks due to the localized surface plasmon resonance. At other wavelengths, TM waves exhibit low transmissivity. In the whole simulation band, the transmission extinction ratio remains above 10, and the peak value reaches 25. We can further improve TM waves' high absorption wavelength range by stacking multiple resonators in the vertical direction or adopting multiple coplanar resonators of different sizes.

## 4. Conclusion

We proposed a polarization sorting metamaterial to achieve TM wave absorption and TE wave transmission simultaneously. We adopted a sandwich structure of cut-wire resonator-dielectric layer-metal grating. The TM wave incident was perfectly absorbed due to the localized surface plasmon resonance at 8.85 μm. The incident TE wave transmitted the metamaterial in the whole simulation band. Therefore, the absorption extinction ratio of our proposed metamaterial reaches 350, and the transmission extinction ratio reaches 425. In addition, we adopt stacked resonators to achieve polarization-selective absorption and transmission with a wide wavelength range of 7.7-10.1 μm. Our proposed polarization sorting metamaterial can bring new ideas for infrared polarization imaging. For example, we can use layered focal planes to obtain real-time information on both polarization directions. Although the transmission extinction ratio of the broadband polarization-selective metamaterial is not very high due to the transmission of TM waves, we can employ polarization sorting metamaterial (top) and polarization-selective absorber (low) bilayer focal planes to achieve real-time full-polarization component imaging with a high extinction ratio and spatial resolution.

**Funding.** National Natural Science Foundation of China (61735018, 61805242); Jilin Scientific and Technological Development Program (20190103014JH); Excellent Member of Youth Innovation Promotion Association of the Chinese Academy of Sciences (2014193, Y201836); Leading Talents and Team Project of Scientific and Technological Innovation for Young and Middle-aged Groups in Jilin Province (20190101012JH).

**Disclosures.** The authors declare no conflicts of interest.

**Data availability.** Data underlying the results presented in this paper are not publicly available at this time but may be obtained from the authors upon reasonable request

## References

1. M. Liu, W. Zhu, P. Huo, L. Feng, M. Song, C. Zhang, L. Chen, H. J. Lezec, Y. Lu, A. Agrawal, and T. Xu, "Multifunctional metasurfaces enabled by simultaneous and independent control of phase and amplitude for orthogonal polarization states," Light: Sci. Appl. **10**(1), 107 (2021).
2. L. Deng, J. Deng, Z. Guan, J. Tao, Y. Chen, Y. Yang, D. Zhang, J. Tang, Z. Li, Z. Li, S. Yu, G. Zheng, H. Xu, C. W. Qiu, and S. Zhang, "Malus-metasurface-assisted polarization multiplexing," Light: Sci. Appl. **9**(1), 101 (2020).
3. R. A. Shelby, D. R. Smith, and S. Schultz, "Experimental Verification of a Negative Index of Refraction," Science **292**(5514), 77–79 (2001).
4. K. Liu, M. Lian, K. Qin, S. Zhang, and T. Cao, "Active tuning of electromagnetically induced transparency from chalcogenide-only metasurface," Light: Adv. Manuf. **2**(0), 1 (2021).
5. C. Chen, W. Song, J. W. Chen, J. H. Wang, Y. H. Chen, B. Xu, M. K. Chen, H. Li, B. Fang, J. Chen, H. Y. Kuo, S. Wang, D. P. Tsai, S. Zhu, and T. Li, "Spectral tomographic imaging with aplanatic metalens," Light: Sci. Appl. **8**(1), 99 (2019).
6. D. Schurig, J. J. Mock, B. J. Justice, S. A. Cummer, J. B. Pendry, A. F. Starr, and D. R. Smith, "Metamaterial Electromagnetic Cloak at Microwave Frequencies," Science **314**(5801), 977–980 (2006).
7. Y. Zhu, Z. Li, Z. Hao, C. DiMarco, P. Maturavongsadit, Y. Hao, M. Lu, A. Stein, Q. Wang, J. Hone, N. Yu, and Q. Lin, "Optical conductivity-based ultrasensitive mid-infrared biosensing on a hybrid metasurface," Light: Sci. Appl. **7**(1), 67 (2018).

Optics EXPRESS


8. N. Liu, M. Mesch, T. Weiss, M. Hentschel, and H. Giessen, "Infrared perfect absorber and its application as plasmonic sensor," Nano Lett. **10**(7), 2342–2348 (2010).
9. N. I. Landy, S. Sajuyigbe, J. J. Mock, D. R. Smith, and W. J. Padilla, "Perfect metamaterial absorber," Phys. Rev. Lett. **100**(20), 207402 (2008).
10. Y. Q. Ye, Y. Jin, and S. He, "Omnidirectional, polarization-insensitive and broadband thin absorber in the terahertz regime," J. Opt. Soc. Am. B **27**(3), 498–504 (2010).
11. K. Aydin, V. E. Ferry, R. M. Briggs, and H. A. Atwater, "Broadband polarization-independent resonant light absorption using ultrathin plasmonic super absorbers," Nat. Commun. **2**(1), 517 (2011).
12. W. Li and J. Valentine, "Metamaterial perfect absorber based hot electron photodetection," Nano Lett. **14**(6), 3510–3514 (2014).
13. Y. Li, D. Li, D. Zhou, C. Chi, S. Yang, and B. Huang, "Efficient, Scalable, and High-Temperature Selective Solar Absorbers Based on Hybrid-Strategy Plasmonic Metamaterials," Sol. RRL **2**(8), 1800057 (2018).
14. A. Lochbaum, Y. Fedoryshyn, A. Dorodnyy, U. Koch, C. Hafner, and J. Leuthold, "On-Chip Narrowband Thermal Emitter for Mid-IR Optical Gas Sensing," ACS Photonics **4**(6), 1371–1380 (2017).
15. W. Ma, Y. Wen, X. Yu, Y. Feng, and Y. Zhao, "Performance enhancement of uncooled infrared focal plane array by integrating metamaterial absorber," Appl. Phys. Lett. **106**(11), 111108 (2015).
16. C. Chen, G. Wang, Z. Zhang, and K. Zhang, "Dual narrowband absorber based on metal-insulator-metal configuration for refractive index sensing," Opt. Lett. **43**(15), 3630–3633 (2018).
17. X. Tan, H. Zhang, J. Li, H. Wan, Q. Guo, H. Zhu, H. Liu, and F. Yi, "Non-dispersive infrared multi-gas sensing via nanoantenna integrated narrowband detectors," Nat. Commun. **11**(1), 5245 (2020).
18. K. Sun, C. A. Riedel, Y. Wang, A. Urbani, M. Simeoni, S. Mengali, M. Zalkovskij, B. Bilenberg, C. H. de Groot, and O. L. Muskens, "Metasurface Optical Solar Reflectors Using AZO Transparent Conducting Oxides for Radiative Cooling of Spacecraft," ACS Photonics **5**(2), 495–501 (2018).
19. N. A. Rubin, G. D'Aversa, P. Chevalier, Z. Shi, W. T. Chen, and F. Capasso, "Matrix Fourier optics enables a compact full-Stokes polarization camera," Science **365**(6448), 1 (2019).
20. W. Li, Z. J. Coppens, L. V. Besteiro, W. Wang, A. O. Govorov, and J. Valentine, "Circularly polarized light detection with hot electrons in chiral plasmonic metamaterials," Nat. Commun. **6**(1), 8379 (2015).
21. J. Wei, C. Xu, B. Dong, C.-W. Qiu, and C. Lee, "Mid-infrared semimetal polarization detectors with configurable polarity transition," Nat. Photonics **15**(8), 614–621 (2021).
22. C. Yan, X. Li, M. Pu, X. Ma, F. Zhang, P. Gao, K. Liu, and X. Luo, "Midinfrared real-time polarization imaging with all-dielectric metasurfaces," Appl. Phys. Lett. **114**(16), 161904 (2019).
23. Z. Lin, Z. Xu, P. Liu, Z. Liang, and Y.-S. Lin, "Polarization-sensitive terahertz resonator using asymmetrical F-shaped metamaterial," Opt. Laser Technol. **121**, 105826 (2020).
24. D. Sood and C. C. Tripathi, "Broadband ultrathin low-profile metamaterial microwave absorber," Appl. Phys. A **122**(4), 332 (2016).
25. M. Parvinnezhad Hokmabadi, D. S. Wilbert, P. Kung, and S. M. Kim, "Polarization-Dependent, Frequency-Selective THz Stereometamaterial Perfect Absorber," Phys. Rev. Appl. **1**(4), 044003 (2014).
26. D. Lee, S. Y. Han, Y. Jeong, D. M. Nguyen, G. Yoon, J. Mun, J. Chae, J. H. Lee, J. G. Ok, G. Y. Jung, H. J. Park, K. Kim, and J. Rho, "Polarization-sensitive tunable absorber in visible and near-infrared regimes," Sci. Rep. **8**(1), 12393 (2018).
27. Y. K. Zhong, S. M. Fu, W. Huang, D. Rung, J. Y. Huang, P. Parashar, and A. Lin, "Polarization-selective ultra-broadband super absorber," Opt. Express **25**(4), A124–A133 (2017).
28. L. Zhang, Y. Zheng, J. Zhang, Y. Yin, Q. Li, J. Lei, and Y. Zhu, "Tunable polarization-sensitive, long-wave infrared MDM subwavelength grating structure with wide-angle, narrow-band, and high absorption," Opt. Express **29**(14), 21473–21491 (2021).
29. J. Li, L. Bao, S. Jiang, Q. Guo, D. Xu, B. Xiong, G. Zhang, and F. Yi, "Inverse design of multifunctional plasmonic metamaterial absorbers for infrared polarimetric imaging," Opt. Express **27**(6), 8375–8386 (2019).
30. B. F. Andresen, G. F. Fulop, C. M. Hanson, P. R. Norton, S. Ogawa, Y. Takagawa, and M. Kimata, "Polarization-selective uncooled infrared sensor using a one-dimensional plasmonic grating absorber," in *Infrared Technology and Applications XLI*, (2015).
31. L. Chen and Z. Song, "Simultaneous realizations of absorber and transparent conducting metal in a single metamaterial," Opt. Express **28**(5), 6565–6571 (2020).
32. T. Wang, H. Zhang, Y. Zhang, Y. Zhang, and M. Cao, "Tunable bifunctional terahertz metamaterial device based on Dirac semimetals and vanadium dioxide," Opt. Express **28**(12), 17434–17448 (2020).
33. T. Wang, Y. Zhang, H. Zhang, and M. Cao, "Dual-controlled switchable broadband terahertz absorber based on a graphene-vanadium dioxide metamaterial," Opt. Mater. Express **10**(2), 369 (2020).
34. T. Wang, H. Zhang, Y. Zhang, and M. Cao, "A bi-tunable switchable polarization-independent dual-band metamaterial terahertz absorber using $VO_2$ and Dirac semimetal," Results Phys. **19**, 103484 (2020).
35. A. D. Rakić, A. B. Djurišić, J. M. Elazar, and M. L. Majewski, "Optical properties of metallic films for vertical-cavity optoelectronic devices," Appl. Opt. **37**(22), 5271–5283 (1998).
36. M. R. Querry, *Optical constants of minerals and other materials from the millimeter to the ultraviolet* (Chemical Research, Development & Engineering Center, US Army Armament . . . , 1987).

Optics EXPRESS

37. D. R. Smith, D. C. Vier, T. Koschny, and C. M. Soukoulis, "Electromagnetic parameter retrieval from inhomogeneous metamaterials," Phys. Rev. E **71**(3), 036617 (2005).
38. J. Hao, J. Wang, X. Liu, W. J. Padilla, L. Zhou, and M. Qiu, "High performance optical absorber based on a plasmonic metamaterial," Appl. Phys. Lett. **96**(25), 251104 (2010).
39. H. A. Macleod and H. A. Macleod, *Thin-film optical filters* (CRC press, 2010).
40. S. Jiang, J. Li, J. Li, J. Lai, and F. Yi, "Metamaterial microbolometers for multi-spectral infrared polarization imaging," Opt. Express **30**(6), 9065–9087 (2022).